Ultra-fast underwater suction traps

Olivier Vincent[a], Carmen Weißkopf[b], Simon Poppinga[b], Tom Masselter[b], Thomas Speck[b], Marc Joyeux[a], Catherine Quilliet[a] and Philippe Marmottant[a,1]

[a] *Laboratoire de Spectrométrie Physique, UMR5588 CNRS - University of Grenoble 1, Avenue de la Physique 140, BP 38047 Saint Martin d'Hères Cedex 02, France*

[b] *Plant Biomechanics Group Freiburg, Botanic Garden, Faculty of Biology, University of Freiburg, Schänzlestrasse 1, D-79104 Freiburg i. Br., Germany*

[1] *To whom correspondence should be addressed. Tel: +33 4 76 51 42 89, Fax: +33 4 76 63 54 95, E-mail: marmotta@spectro.ujf-grenoble.fr*

Abstract

Carnivorous aquatic *Utricularia* species catch small prey animals with millimeter-sized underwater suction traps, which have fascinated scientists since Darwin's early work on carnivorous plants. Suction takes place after mechanical triggering and is due to a release of stored elastic energy in the trap body, accompanied with a very fast opening and closure of a trapdoor which otherwise closes the trap entrance watertight. The exceptional trapping speed far above human visual perception impeded profound investigations up to now. Using high-speed video imaging and special microscopy techniques, we obtained fully time-resolved recordings of the door movement. We found that this unique trapping mechanism conducts suction in less than a millisecond and therefore ranks among the fastest plant movements known. Fluid acceleration reaches very high values, leaving little chances for prey animals to escape. We discovered that the door deformation is morphologically predetermined, and actually performs a buckling/un-buckling process including a complete trapdoor curvature inversion. This process, that we predict using dynamical simulations and simple theoretical models, is highly reproducible: the traps are autonomously repetitive as they fire spontaneously after 5-20 hours and reset actively to their ready-to-catch condition.

Keywords: bladderwort, carnivorous / insectivorous plants, suction mechanism, functional morphology, fluid dynamics

Introduction

Bladderworts (*Utricularia spp*., Lentibulariaceae) are carnivorous as an adaptation to nutrient-poor habitats (1-4). The genus comprises more than 220 species with an almost worldwide distribution and exhibits different life-forms (4, 5). Probably as the most extreme embodiment of the carnivorous syndrome (3) all species are completely rootless and feature a suction trap mechanism which relies on a release of stored elastic energy in the trap body. Entailing a cascade of fast motions (6-15), the whole trapping action is too fast to be followed with the naked eye. Yet, there are no detailed camera recordings available, and the exact motion pattern is unclear up to now. In order to understand how the trap door opens, and to elucidate the dynamics of the motion sequences involved, we studied traps of three aquatic species: *Utricularia australis* L., *U. inflata* WALTER and *U. vulgaris* L. All species belong to the infrageneric section *Utricularia* (5, 16), which shows, as far as known, a homogeneous trap architecture (17) with - as to its functional morphology - a nearly identical trapping mechanism. Trap diameters range from 0.5–3 mm (5, 17).

The lenticular *Utricularia* trap (Fig. 1*A* and S1) works with a two-phase mechanism (2, 3). During the first slow phase, which lasts about 1 hour, internal glands actively pump water out of the trap interior, so that elastic energy is stored in the trap body due to a lower internal hydrostatic pressure. In this set-condition, when ready for catch, the trap shows concave wall curvatures. A flexible door with protruding trigger hairs closes the entrance watertight. Prey animals can stimulate these hairs and thereby launch the second, ultra-fast phase, which runs passively due to a mechanical conversion of elastic energy into kinetic energy. The triggering results in door opening, trap wall relaxation and water (and thereby prey) influx due to the sudden increase of the trap volume. After the door is closed, the prey is dissolved by digestive enzymes (secreted by quadrifid glands), and nutrients are absorbed by the plant. Both phases together form a repeatable 'active slow deflation/passive fast suction' sequence (Fig. 1*B*) (Movie S1 and S2).

Materials and Methods

Experiments We investigated traps (2–3 mm in diameter) of the species *U. inflata, U. vulgaris* and *U. australis*. The motion was studied with a high-performance light-microscope (Olympus IX70) and stereo microscopes (Zeiss DV8, Olympus SZX9, up to x85.5). Trapping actions were recorded with up to 15000 frames per second (high-speed cameras Phantom

Miro 4, Vision Research, and I-Speed 3, Olympus). Particles used to track the flow were hollow glass spheres with a diameter in the 2-20 μm range and a density of 1.1 g/cm^3 (Polysciences, Inc.). Laser sheet fluorescence microscopy (18) was used to observe directly the median trapdoor axis (laser sheet about 10 μm thick) of a trap, previously infused in rhodamine dye for a few minutes. Scanning electron microscopy (SEM) imaging involved the following preparation steps: dehydration of specimen with methanol substitution, critical-point drying with a Bal-Tec CPC 030 and gold-coating (~15nm) with a Cressington Sputter Coater 108 auto. The SEM LEO 435 VP was used.

Time Measurements The different steps during trapdoor opening in *U. inflata* and *U. vulgaris* were found to vary in duration. We recorded 16 openings with at least 3000 fps. 1) Buckling (see Results and Discussion) duration varied between 0.7 ms and 21 ms (2 ms on average). We interpret this wide range to be due to variations in pressure values before triggering or different frictions on the threshold. 2) Opening lasts between 0.4 ms and 0.8 ms (0.5 ms on average). 3) The closure took between 1 ms and 5.5 ms (2.5 ms on average), with a small proportion of curvature remaining. Final resetting of the trap door took between 0.5 ms and 300 ms.

Elastic shell simulations. The trap body and trapdoor are modelled as elastic shells of thickness h, Young modulus of elasticity E, and Poisson ratio ν. Their potential energy U_{pot} is the sum of a bending term, U_{bend} , and a stretching term, U_{stretch} (19):

$$U_{\text{bend}} = \frac{Eh^3}{24(1-\nu^2)} \int_S [(\text{Tr}(\mathbf{b}))^2 - 2(1-\nu)\text{Det}(\mathbf{b})]\, dS, \qquad (1)$$

$$U_{\text{stretch}} = \frac{E\,h}{2(1-\nu^2)} \int_S [\nu(\text{Tr}(\boldsymbol{\varepsilon}))^2 + (1-\nu)\text{Tr}(\boldsymbol{\varepsilon}^2)]\, dS, \qquad (2)$$

with $\mathbf{b}$ as the difference between the strained and unstrained local curvature tensors and $\boldsymbol{\varepsilon}$ as the 2D Cauchy-Green local strain tensor. The integrals are evaluated on the surface S of the shell. It is assumed that the material is incompressible, which implies $\nu = 0.5$. All surfaces are described as triangular meshes (Fig. 2A).

The body of the *Utricularia* trap is modelled as a closed shell with a realistic shape (larger radius 1 mm, thickness h=h_{body}=60 μm). The initial shape holds a portion of surface with negative curvature (Fig. 1), ensuring a smooth deflation. Simulations are performed by decreasing quasi-statically the inner volume V, and by searching for each volume the geometry that minimizes the potential energy U_{pot} using Surface Evolver freeware (20). The

pressure difference Δp between the inside and the outside of a trap is expressed by $\Delta p = -\mathrm{d}(\min(U_{\mathrm{pot}}))/\mathrm{d}V$. The Young modulus $E=E_{\mathrm{body}}$ is determined by requiring the inner volume V to be reduced by about 40% for Δp=15 kPa (12, 14).

The *Utricularia* trapdoor is modelled as a quarter of a prolate ellipsoid, with a polar radius of 300 μm and an equatorial radius of 240 μm, the pole axis joining the sides of the trap, and a thickness h_{door}=30 μm (see Fig. 4*D-F*). One of the borders of the ellipsoid represents the trapdoor frame and is kept fixed, whereas the lower edge is free to move. During the dynamic simulation, the pressure inside the trap is slowly decreased from atmospheric pressure, and the position $\mathbf{r}_k$ of each vertex k of the mesh is updated according to a Langevin equation

$$m_k \frac{d^2\mathbf{r}_k}{dt^2} = -\nabla U_{\mathrm{pot}} - \Delta p\, \delta A_k \mathbf{n}_k - m_k \gamma \frac{d\mathbf{r}_k}{dt} + \sqrt{2 m_k \gamma k_{\mathrm{B}} T}\, \frac{dW(t)}{dt}, \qquad (3)$$

with m_k as the mass of the vertex, δA_k as the element of surface that surrounds vertex k, $\mathbf{n}_k$ as the outward normal to the surface, k_{B} the Boltzmann constant, T the ambient temperature, and $W(t)$ as a Wiener process. The first and second term in the right-hand side of this equation describe elastic and pressure forces, respectively, while the two last terms model the effects of the liquid, namely friction and thermal noise, even if the full motion of the fluid around the trap is not modeled. The dissipation coefficient γ is assumed to be $2\mathrm{x}10^5$ s^{-1}. Thermal noise happens to be orders of magnitude smaller than elastic forces, and was introduced for the sake of completeness**.** A constant pressure difference is imposed in order to model the first phase of opening (after full opening the pressure difference relaxes). When assuming $E_{\mathrm{door}} = 2.7$ MPa, one observes that the shape of the door remains essentially unchanged up to Δp=15.5 kPa.

Full detail of these simulations will be provided in a separate paper.

Prediction of pressure for door buckling Using scaling arguments, the buckling pressure of a spherical shell (21) is approximately given by:

$$P_{\mathrm{buckling}} \sim E_{\mathrm{door}} \left(\frac{h_{\mathrm{door}}}{R_{\mathrm{door}}} \right)^2, \qquad (4)$$

with R_{door} the typical radius of curvature of the door and h_{door} the thickness of the door.

Prediction of the duration of trap inflation The trap is mechanically equivalent to a mass-spring system, initially under compression, that is suddenly released. The spring to consider

arises from the elasticity of the trap body, and its stiffness k resulting from the force squeezing the sides $k\Delta e = S\,\Delta p$, with Δe=0.5 mm as the change in width and S=1 mm^2 as the area of each side. The mass m_a is that of the displaced fluid, which is comparable to the total mass of fluid in the trap after firing (volume in the order of 1mm^3). This mass-spring system relaxes with a characteristic inertial time $\tau = 2\pi(m_a/k)^{1/2}$=1 ms, comparable to the recorded time of suction (1 ms).

Results and Discussion

Although the first phase (active slow deflation) has already been documented in terms of deflated volume and internal pressure (12), the elastic shell simulations presented here allow estimating the stiffness of the trap body. The trap body is characterized by a Young's modulus in the range of 5-20 MPa (Fig. 2) (Movie S3), which is in the range of that of fully turgescent parenchymatous tissues (22). It is two cell-layers thick, mostly flexible and therefore supports the deflation phase.

The second phase comprises trap wall relaxation and trapdoor opening/closure. We investigated suction dynamics and trapdoor movement, using high speed video imaging with up to 15000 frames per second, and digital particle tracking. Capture of small crustaceans (freshwater copepods of the genus *Cyclops*) were recorded. Caught animals loop within the traps, indicating that swirls develop inside (Fig 3*A*) (Movie S4). We hypothesize that these swirls, despite not being investigated here, are crucial for prey retention and due to the inner trap structure. The trapping sequence itself lasts a few milliseconds only. The time span of suction itself is half a millisecond, which is much shorter than previously estimated (3, 12). *Utricularia* therefore features the fastest trapping movement of all carnivorous plants, ranking even among the fastest movements generally known in plant kingdom (23-27). The suction time after trap door opening can be estimated with simple arguments based on the trap body elasticity and the mass of water displaced, see Methods. The fluid speed was deduced by tracking small glass beads (Fig. 3*B* and *C*). We recorded a maximum fluid velocity of 1.5 m/s, implying that liquid inertia forces are well above viscous forces (the ratio of these forces, the Reynolds number, reaches 900), and measured a maximum fluid acceleration of 600 *g*.

The swiftness of the suction is enabled by the extremely fast opening and closure of the door, which acts as a flexible valve (2, 9, 10). Our high-speed video recordings in fluorescence laser

sheet microscopy reveal the following sequence (Fig. 3*B and D*) (Movie S5-S7) after manually triggering the trap with a fine needle: 1) Inversion of the door curvature. The convex trapdoor - in the 'ready-to-catch condition' - bulges inside, starting at the region of trigger hair insertion. This inversion of curvature then spreads progressively over the door surface (Fig. 4*A* and *B*), with the door still being closed. In this phase the trigger hairs converge and flap against the door, so they do not block the trap entrance during step two. 2) Opening. The door swings inside rapidly (Fig. 4*C*), in about 0.5 ms on average. 3) Door resetting. The door quickly moves back in about 2.5 ms on average. A large proportion of inverted curvature remains, then disappears as the door gets back to its initial position. The duration for a total curvature resetting may be as fast as 0.5 ms, or lasts up to 300 ms in some cases.

The fast door opening and closure, with an abrupt change in shape, strongly suggests that the underlying principle is a buckling (23) of an elastic valve. We hypothesize that, after the trap is set, the internal/external pressure difference is close to the critical pressure for spontaneous buckling, and a slight disturbance suffices to trigger the motion. The triggering could be entirely mechanical (trigger hairs acting as levers) (2, 9), but we cannot exclude an excitatory step (physiological sensitivity) that would help exceeding the remaining mechanical activation barrier (12). The door buckles prior to opening, contrary to the previous assumption stating that opening starts before buckling (2, 9). After trap inflation the inside and outside pressures are levelled, and the door un-buckles to its initial state of curvature, thereby closing the trap. Note that such large door displacements involve relatively small surface strains of the door: it can be estimated that the longitudinal strain of the outer surface is $-h_{door}/R_{door}=-0.1$ when achieving full curvature inversion, and the opposite for the inner surface.

This buckling hypothesis is well supported by our dynamic simulations. We modelled the *Utricularia* door as a quarter-ellipsoidal shell (see Methods). One border of the ellipsoid is fixed, whereas the other border (free edge) is in frictionless contact with a threshold. The shell has both bending and stretching energy. We performed dynamics simulations whilst the pressure inside the trap was slowly decreased. We noticed that the door shape changes very little up to a pressure difference of 15.5 kPa. Buckling then spontaneously occurs, with the door sliding along the threshold and swinging open, in excellent concordance with our high-speed videos of the actual trapdoor (Fig. 4*D–F*) (Movie S8). When the pressure difference is just lower than this critical value the trap is stable, but the energy barrier to trigger buckling is low, making the trap extremely sensitive to external perturbation.

Independently from simulations, the buckling mechanism entails a general estimation for door and body wall thicknesses in *Utricularia*. The doors should be thin enough so that they buckle due to underpressure generated by active pumping water out of the trap. Furthermore, we can hypothesize that, in order to suck a maximum amount of water and thereby prey, mechanical and geometrical parameters of the body walls and the door should be optimized so that the body reaches a nearly whole deflation at the opening pressure. A too stiff body would not deform enough, and hence suck a too small amount of water, while a too soft body would hardly overcome viscous dissipation and then not be fast enough during entrapping suction. The elastic energy at a maximum deflation, in the order of $E_{\text{body}}\, h_{\text{body}}^3$ (according to Eq. 1, using a deformation of relative amplitude 1) therefore should be equal to the work generated by pressure at buckling, in the order of $P_{\text{buckling}}\, R^3$, with R the typical size of the trap. Using the scaling expression for the buckling pressure (Eq. 4), we predict the following door to body thickness ratio:

$$\frac{h_{\text{door}}}{h_{\text{body}}} \sim \left(\frac{h_{\text{body}}}{R}\right)^{1/2}\left(\frac{E_{\text{body}}}{E_{\text{door}}}\right)^{1/2} . \quad (5)$$

Such a ratio is smaller than one, because the thickness h_{body} is much smaller than the size of the trap R, and because the range of Young's moduli for parenchymatous tissues does not extend over several orders of magnitude. We therefore conclude that doors of aquatic *Utricularia* are thinner than their body, in order to open at a maximum deflation. This result should be important for the consideration of trap functioning in other *Utricularia* species where the suction mechanism is doubtful, e.g. in the terrestrial *U. multifida* (17).

Furthermore, we found that aquatic *Utricularia* traps can fire spontaneously, corroborating a hypothesis reported in (28), by continuously imaging a single trap during 20 days. We observed more than 60 successive spontaneous suctions during this time span, assuming that tiny swimming organisms like algae are not capable of triggering the mechanism (29). Traps activate on average at time intervals between 5 h and 20 h (Fig. S2) (Movie S2). This observation (also reported by 30) confirms the buckling scenario: the pressure inside the trap reaches a low value that entails buckling, most likely due to mechanical/thermal noise.

Looking in detail at the trapdoor morphology, we found how it is optimized for fast buckling and un-buckling. The roughly semi-circular door is fixed to the upper part of the trap entrance along a curved arch. It rests with its free edge on the lower part of the entrance, i.e. the threshold (Fig. S1). Here, mucilage is secreted, and in combination with an exfoliated cuticle (velum) a watertight seal is achieved (2, 3). We noticed that the free edge of the door always

features two conspicuous lateral folds (Fig. 5), which presumably add displacement space by unfolding.

The trapdoor consists of two differing cell layers. Those of the inner layer are elongated and radially arranged around the central hinge region (Fig. 5*A*). The most noticeable feature is the pattern of concentric circular lines, indicating constrictions of the cells in this middle region. These cells have been assumed to function like compressive bellows (2, 3). In addition, considering the observed deformation, we suggest that these constrictions act as pre-folds, increasing flexibility in the radial direction. This would channel the reversible buckling/unbuckling process and enforce it to follow the same reproducible deformation pattern. Buckling starts in the thickened middle piece below the thin central hinge region, resulting in trigger hair converging and flapping against the door. The hinge region along the curved arch is characterized by radially arranged cells without constrictions. This region is less affected by deformation and might serve as a spring-like structure for closing the door. In contrast, the outer cell layer of the door is not distinctly compartmentalized and features smaller cells, running parallel to each other (Fig. 5*B*).

In conclusion, our investigations show how buckling and un-buckling lead to door opening and closure, which is associated with a suction swirl. This differs from mechanism of the Venus Flytrap (*Dionaea muscipula)*, described as snap-buckling (26) where a one-way only internal buckling results in the trapping movement. The remarkable valve mechanism of *Utricularia* should provide inspiration for a great variety of biomimetic applications, especially for new deployable materials and fluid-elastic structures designed to act repeatedly, such as in microfluidic devices. On a biological level, the repetitive spontaneous valve buckling and opening could account for reports on phytoplankton, bacterial communities and detritus regularly found in traps (28, 29, 31, 32). Usually considered as 'bycatch', there is evidence that they play an important role in *Utricularia* nutrient supply (31-35). The evolutionary success of these carnivorous plants might be explained by the fact that their traps are not only active, but also autonomous: this character could facilitate the rootless *Utricularia* plants to colonize nutrient-poor habitats.

Acknowledgements

P. M. wishes to thank Clément Nizak for his help in setting the Laser sheet fluorescence microscopy set-up. S.P. would like to thank Lubomir Adamec, Trebon (Czech Republic), for providing plant material.

References:

1. Darwin, C. 1875 *Insectivorous plants*. London: Murray.
2. Lloyd, F. E. 1942 *The carnivorous plants*. Massachusetts: Waltham.
3. Juniper, B. E., Robins, R. J., Joel, D. M. 1989 *The carnivorous plants*. London: Academic.
4. Barthlott, W., Porembski, S., Seine, R., Theisen, I. 2008 *The curious world of carnivorous plants: a comprehensive guide to their biology and cultivation*. Portland: Timber.
5. Taylor, P. 1989 *The genus Utricularia: a taxonomic monograph*. London: Kew Bull Add Ser XIV.
6. Treat, M. 1875 Is the valve of *Utricularia* sensitive? *Harper's New Monthly Magazine* 52, 382-387.
7. Czaja, A. T. 1922 Die Fangvorrichtung der Utriculariablase. *Z Bot* 14, 705-729.
8. Ekambaram, T. 1924 Note on the mechanism of the bladders of *Utricularia*. *J Indian Bot Soc* 4, 73-74.
9. Lloyd, F. E. 1932 Is the door of *Utricularia* an irritable mechanism? *Can J Bot* 10, 780–786.
10. Lloyd, F. E. 1929 The mechanism of the water tight door of the *Utricularia* trap. *Plant Physiol* 4, 87–102.
11. Diannelidis, T., Umrath, K. 1953 Aktionsströme der Blase von *Utricularia vulgaris*. *Protoplasma* 42, 58-62.
12. Sydenham, P., Findlay, G. 1973 The rapid movement of the bladder of *Utricularia sp*. *Aust J Biol Sci* 26, 1115-1126.
13. Withycombe, C. L. 1924 On the function of the bladders of *Utricularia*. *J Linn Soc* 46, 401-413.
14. Sasago, A., Sibaoka, T. 1985 Water extrusion in the trap bladders of *Utricularia vulgaris*. I. A possible pathway of water across the bladder wall. *Bot Mag, Tokyo* 98, 55-66.
15. Sasago, A., Sibaoka, T. 1985 Water extrusion in the trap bladders of *Utricularia vulgaris*. II. A possible mechanism of water outflow. *Bot Mag, Tokyo* 98, 113-124.
16. Müller, K., Borsch, T. 2005 Phylogenetics of *Utricularia* (Lentibulariaceae) and molecular evolution of the trnK intron in a lineage with high substitutional rates. *Plant Syst Evol* 250, 39–67.

17. Reifenrath, K., Theisen, I., Schnitzler, J., Porembski, S., Barthlott, W. 2006 Trap architecture in carnivorous *Utricularia* (Lentibulariaceae). *Flora* 201, 597-605.
18. Reynaud, E. G., Krzic, U., Greger, K., Stelzer, E. H. K. 2008 Light sheet-based fluorescence microscopy: more dimensions, more photons, and less photodamage. *HFSP J* 2, 266–275.
19. Komura, S., Tamura, K., Kato, T. 2005 Buckling of spherical shells adhering onto a rigid substrate. *Eur Phys J* E 18, 343-358.
20. Brakke, K. 1992 The surface evolver. *Exp Math* 1, 141–165.
21. Landau, L. D., Lifshitz, E. M. 1986 Theory of Elasticity. Oxford: Pergamon.
22. Niklas, K. J. 1988 Dependency of the tensile modulus on transverse dimensions, water potential, and cell number of pith parenchyma. *Am J Bot* 75(9), 1286-1292.
23. Skotheim, J. M., Mahadevan, L. 2005 Physical limits and design principles for plant and fungal movements. *Science* 308, 1308–1310.
24. Edwards, J., Whitaker, D., Klionsky, J., Lasbowski, M. L. 2005 A record breaking pollen catapult. *Nature* 435(12), 164.
25. Nicholson, C. C., Bales, J. W., Palmer-Fortune, J. E., Nicholson, R. G. 2008 Darwin's bee-trap. The kinetics of *Catasetum*, a New World orchid. *Plant Signal Behav* 3(1), 19-23.
26. Forterre, Y., Skotheim, J. M., Dumais, J., Mahadevan, L. 2005 How the Venus Flytrap snaps. *Nature* 433(27), 421-425.
27. Taylor, P. E., Card, G., House, J., Dickinson, M. H., Flagan, R. C. 2006 High-speed pollen release in the white mulberry tree, *Morus alba* L. Sex Plant Reprod 19, 19-24.
28. Peroutka, M., Adlassnig, W., Volgger, M., Lendl, T., Url, W. G., Lichtscheidl, I. K. 2008 *Utricularia*: a vegetarian carnivorous plant? *Plant Ecol* 199(2), 153-162.
29. Alkhalaf, I., Hübener, T., Porembski, S. 2009 Prey spectra of aquatic *Utricularia* species (Lentibulariaceae) in Northeastern Germany: the role of planktonic algae. *Flora* 204(9), 700-708.
30. Adamec, L. 2010 The comparison of mechanically stimulated and spontaneous firings in traps of aquatic carnivorous *Utricularia* species. *Aquat Bot* (2010), doi:10.1016/j.aquabot.2010.09.004.
31. Gordon, E., Pacheco, S. 2007 Prey composition in the carnivorous plants *Utricularia inflata* and *U. gibba* (Lentibulariaceae) from Paria Peninsula, Venezuela. *Rev Biol Trop (Int J Trop Biol ISSN-0034-7744)* 55(3-4), 795-803.

32. Albert, V. A., Jobson, R. W., Michael, T. P., Taylor, D. J. 2010 The carnivorous bladderwort (*Utricularia*, Lentibulariaceae): a system inflates. *J Exp Bot* 61(1), 5-9.
33. Sirova, D., Adamec, L., Vrba, J. 2003 Enzymatic Activities in Traps of Four Aquatic Species of the Carnivorous Genus *Utricularia*. *New Phytol* 159(3), 669-675.
34. Sirova, D., Borovec, J., Santruckova, H., Santrucek, J., Vrba, J., Adamec, L. 2009 *Utricularia* carnivory revisited: plants supply photosynthetic carbon to traps. *J Exp Bot* 61, 101-105.
35. Sirova, D., Borovec, J., Cerna, B., Rejmankova, E., Adamec, L., Vrba, J. 2009 Microbial community development in the traps of aquatic Utricularia species. *Aquat Bot* 90, 129–136.

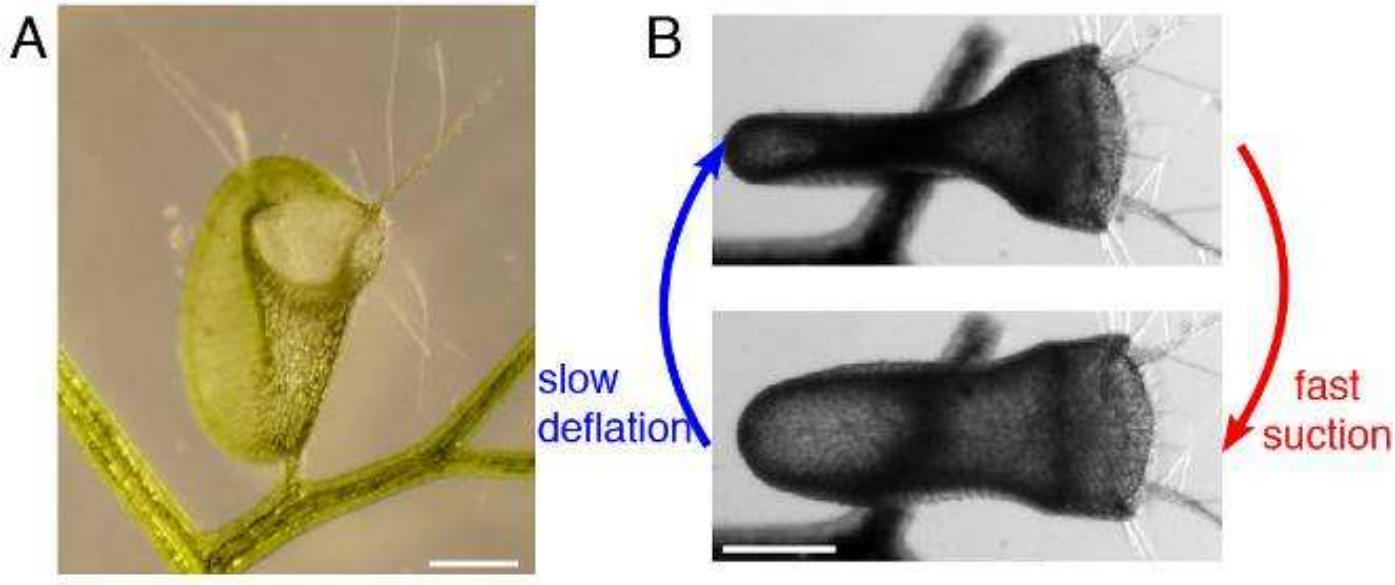

Fig. 1. Traps of *U. inflata*. (*A*) Frontal view of a trap, the concave walls and the entrance are clearly visible. (*B*) Top views of a trap (the door facing to the right) before and after firing, showing the two-phase trap mechanism. The scale bar in all figures is 500 μm.

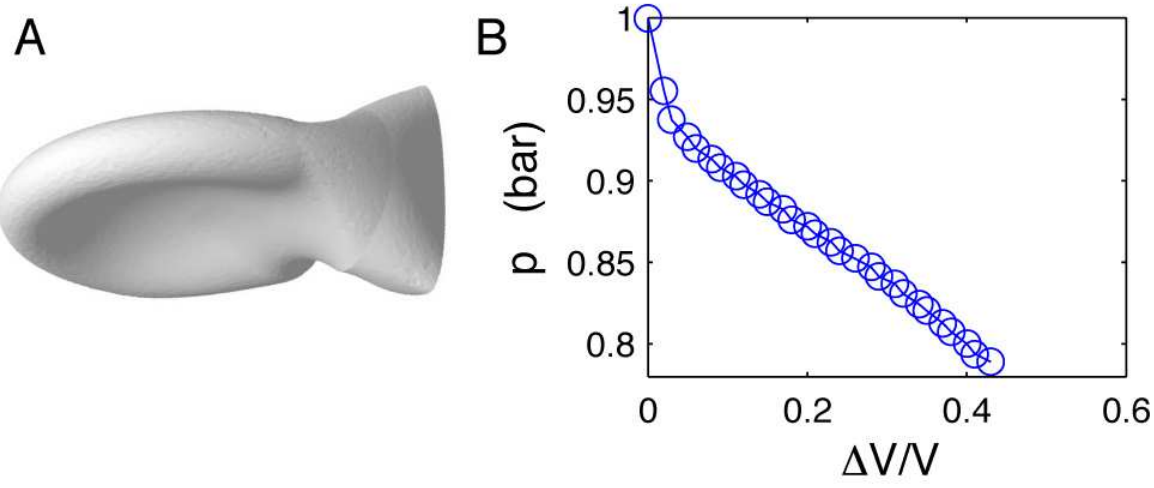

Fig 2. Simulated trap body and pressure values. (*A*) Simulation of the *U. inflata* trap body (the entrance facing rightwards) as an elastic shell, assuming the initial shape of the swollen trap. Due to water removal its sides become concave. The door is not modeled. (*B*) Pressure inside of the *U. inflata* trap as a function of deflation, as computed in simulations. The Young's modulus of the shell is E = 20 MPa, the shell thickness is h = 60 μm, and the largest radius 1 mm.

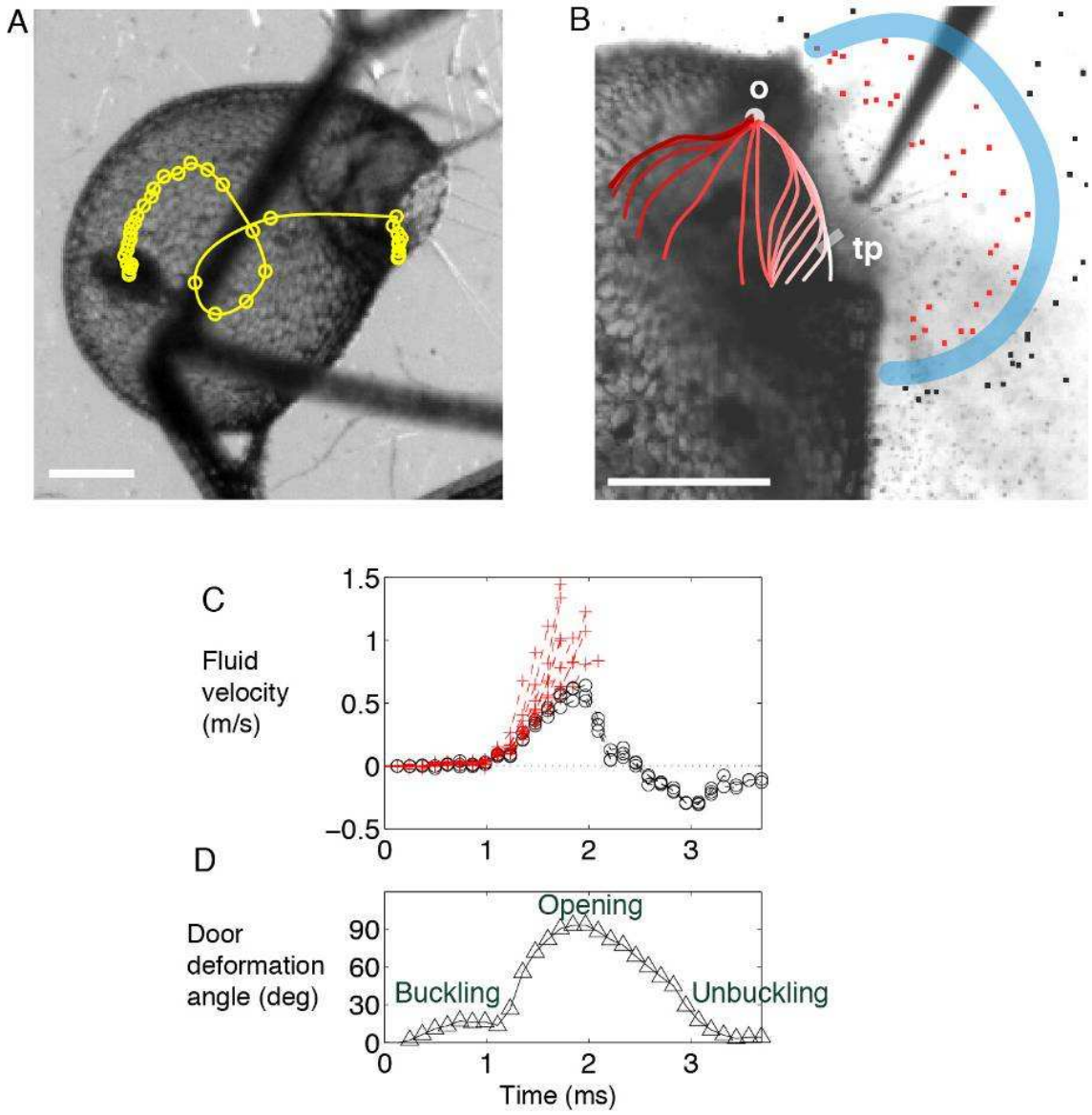

Fig. 3. Suction dynamics in *U. inflata*. (*A)* Fast suction of a small crustacean (*Cyclops spec.*): the circles denote the position of its centre at time intervals of 0.34 ms. (*B*) Detail of the valve profile before suction (side view), with tracer particles suspended in the fluid. The thick blue line delimitates the aspiration zone: only particles within the zone (tagged in red) are 'trapped'. Manual triggering is performed with a needle. We also superimposed a sketch of the median door axis progression during firing, as observed in video images (see also Fig. 4). The progression is displayed using different red scale values, with the lightest white value indicating the initial profile. Each step depicts a 0.34 ms time lag The scale bar is 500 μm. tp, trigger hair insertion point; o, pivot point (see also D). (*C*) Influx velocity of tracer particles. Red crosses indicate 'trapped' particles. Lines are interrupted at trap entrance. (*D*) Temporal angular change of the trigger hair insertion point (tp) during door firing, with the pivot point (o), in relation to its original position when the trap is set. The scale bar in all figures is 500 μm.

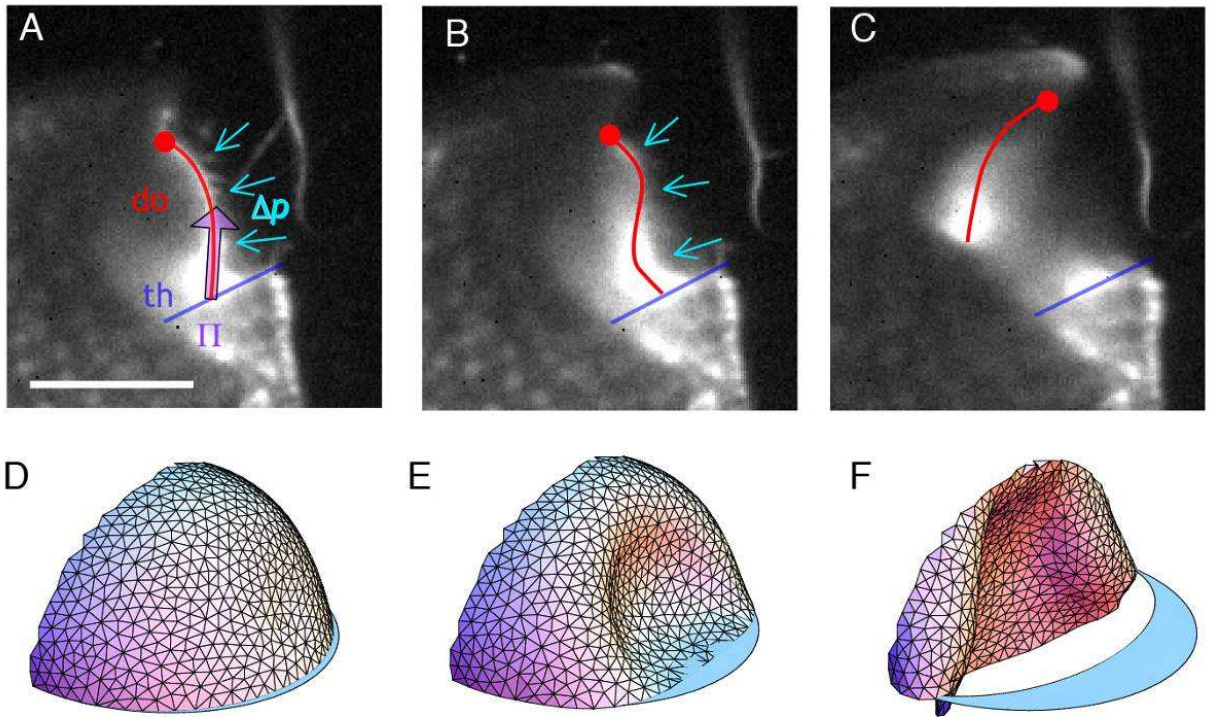

Fig. 4. Inversion of trapdoor curvature in *U. inflata* (*A*)-(*C*). Buckling of the median door axis, visualized by light sheet fluorescence microscopy. (*A*) Initially the trapdoor is convex towards the outside of the trap. The force exerted on the door surface due to water pressure difference Δp between the interior of the trap and the outer medium is balanced by the friction force Π exerted by the threshold (th) on the trapdoor (do). (*B*) Following excitation, the trapdoor becomes gradually concave on its outer side, starting at the trigger hair insertion point. The free edge of the trapdoor is pulled away from the threshold contact area by water pressure. (*C*) Consequently, the door opens wide. (*D*)-(*F*) Dynamic simulation of the trapdoor. Figs. D and E correspond to Figs. A and B, respectively, while Fig. F shows the door only half-way from complete inversion. The scale bar is 500 μm.

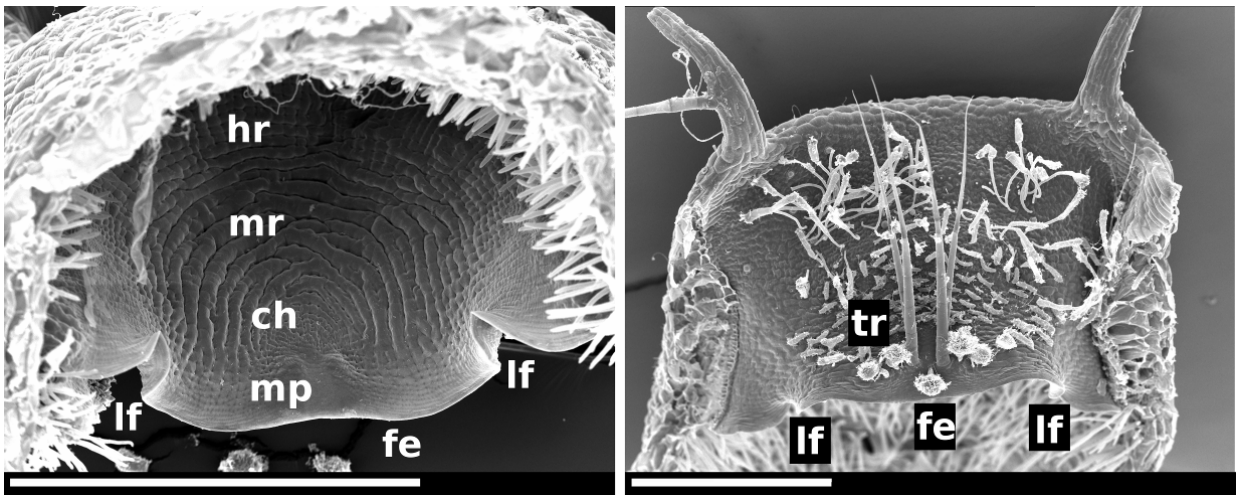

Fig. 5. SEM micrographs of dissected *U. vulgaris* trapdoors. The lateral folds are clearly visible. ch, central hinge; fe, free edge; lf, lateral fold; hr, hinge region; mp, middle piece; mr, middle region; tr, trigger hairs. (*A*) Interior view. (*B*) Exterior view. The scale bar in both figures is 500 μm.

Electronic supplementary material (ESM)

Supplementary figures

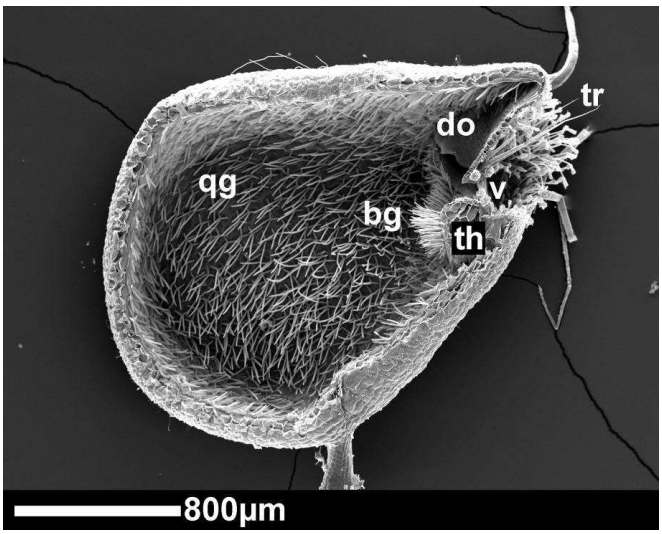

Fig. S1: Longitudinal section of an *U. vulgaris* trap, the door facing rightwards. bg, bifid (internal) glands; do, door; qg, quadrifid glands; th, threshold; tr, trigger hairs; v, velum.

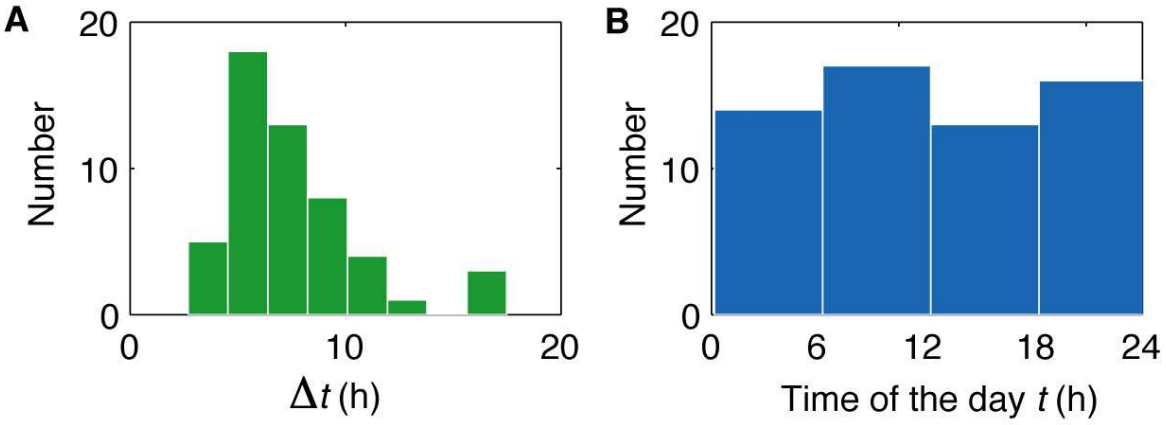

Fig. S2: Distribution of time intervals between spontaneous firing and occurence of spontaneous firing during the day. (A) Time intervals between spontaneous firings of an *U. inflata* trap, held under constant conditions. (B) Numbers of firing events along the day, showing no correlation with daily activity.

Movies

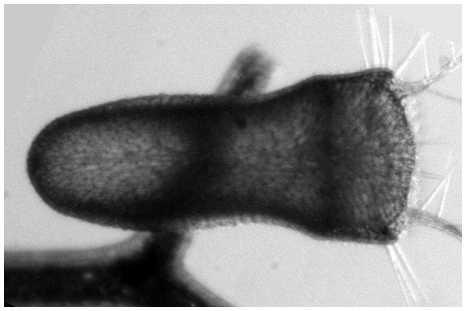

Movie S1: Time lapse recording of an *U. inflata* trap, in top view, showing the trap resetting. The video sequence is 5.5 hours real-time and accelerated 4800 times. At the end both side walls of the trap are almost in contact (QuickTime, 1.8 MB).

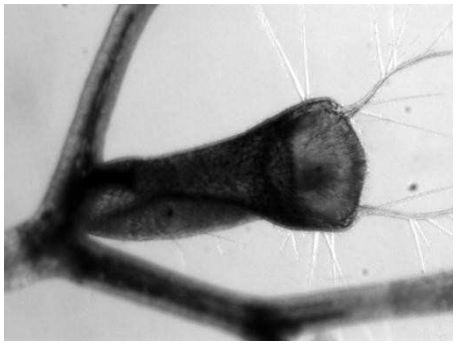

Movie S2: Time lapse recording of an *U. inflata* trap, showing the spontaneous firings and the 'active slow deflation / passive fast suction' sequence. Small particles (primarily phytoplankton) float in the liquid but are supposed to be too small to trigger the trap. The video sequence is 60 hours real-time and accelerated 9000 times (QuickTime, 5.6 MB)

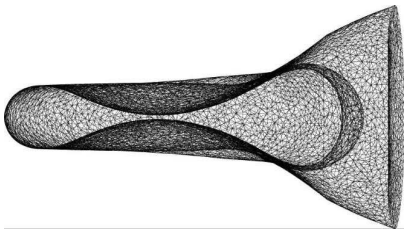

Movie S3: Elastic shell simulation of the trap body, top view, showing the deflation until both opposite trap walls are almost in contact. The trap volume is imposed and the pressure is calculated at each step (QuickTime, 0.8 MB).

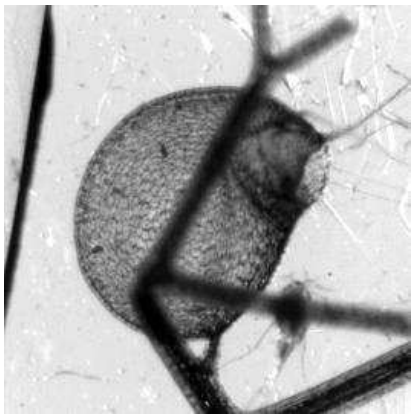

Movie S4: Trap of *U. inflata* catching a small crustacean (copepod of the genus Cyclops), recorded with 1440 fps (frames per second) and played in slow motion at 20 fps (QuickTime, 1.6 MB).

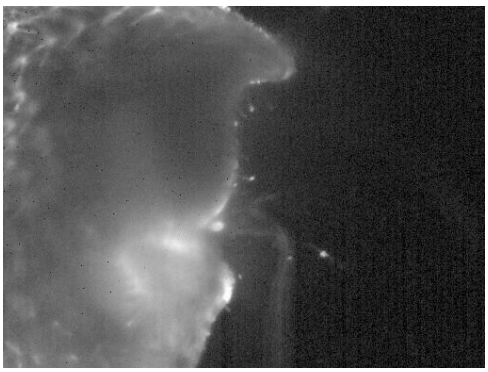

Movie S5: Laser sheet imaging of the trapdoor opening of *U. australis*, recorded with 2900 fps and played with 5 fps (QuickTime, 2 MB).

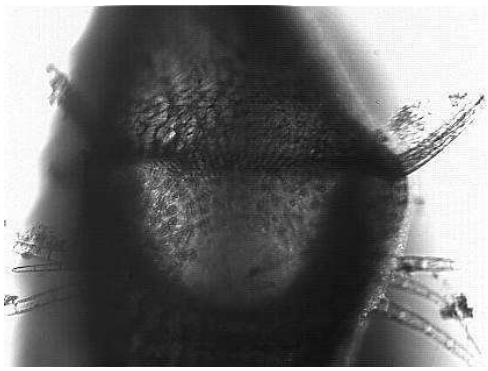

Movie S6: Frontal view on the trapdoor of *U. vulgaris*, the convergence of the trigger hairs is visible. The door does not completely close again. Recorded with 15000 fps and played with 10 fps (QuickTime, 5 MB).

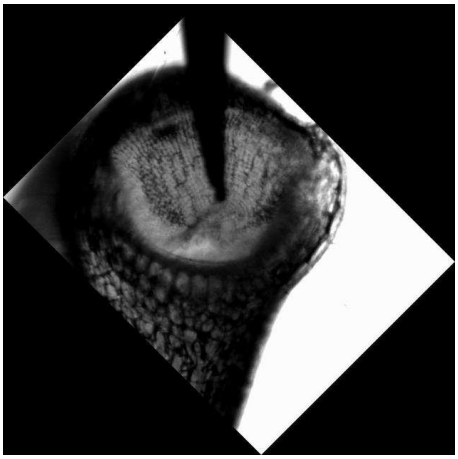

Movie S7: Frontal view on the trapdoor of *U. inflata*, opening and closing (buckling / un-buckling) of the valve is clearly visible, recorded with 2900 fps and played with 10fps (QuickTime, 3.5 MB).

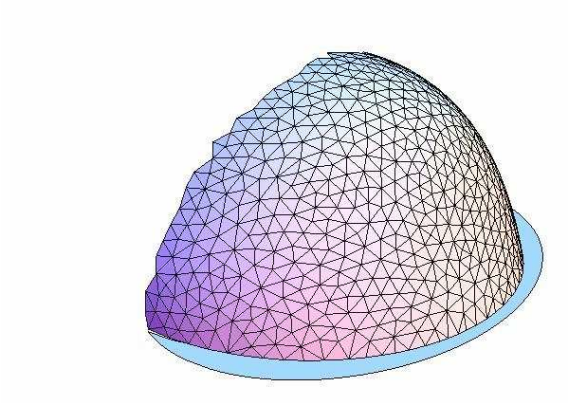

Movie S8: Dynamics simulation of trapdoor opening, at the time when the pressure difference Δp is increased from 15 to 16 kPa. The sequence lasts about 0.5 ms (QuickTime, 7 MB).